Downloaded from jnm.snmjournals.org by on March 14, 2017. For personal use only.

Tumor Localization of 16β-^{18}F-Fluoro-5α-Dihydrotestosterone Versus ^{18}F-FDG in Patients with Progressive, Metastatic Prostate Cancer

Steven M. Larson, MD[1]; Michael Morris, MD[2]; Ilonka Gunther, PhD[1]; Brad Beattie, BA[1]; John L. Humm, PhD[3]; Timothy A. Akhurst, MD[1]; Ronald D. Finn, PhD[1]; Yusuf Erdi, PhD[3]; Keith Pentlow, MS[3]; Jon Dyke, PhD[3]; Olivia Squire, RN[1]; William Bornmann, PhD[1]; Timothy McCarthy[4]; Michael Welch, PhD[4]; and Howard Scher, MD[2]

[1]Department of Radiology, Memorial Sloan-Kettering Cancer Center, New York, New York; [2]Department of Medicine, Memorial Sloan-Kettering Cancer Center, New York, New York; [3]Department of Medical Physics, Memorial Sloan-Kettering Cancer Center, New York, New York; and [4]Mallinckrodt Institute, Washington University School of Medicine, St. Louis, Missouri

This trial was an initial assessment of the feasibility, in vivo targeting, and biokinetics of 16β-^{18}F-fluoro-5α-dihydrotestosterone (^{18}F-FDHT) PET in patients with metastatic prostate cancer to assess androgen receptor expression. **Methods:** Seven patients with progressive clinically metastatic prostate cancer underwent ^{18}F-FDG and ^{18}F-FDHT PET scans in addition to conventional imaging methods. Three patients had their studies repeated 1 mo later, 2 while on testosterone therapy, and the third after treatment with 17-allylamino-17-demethoxygeldanamycin (17-AAG). High-pressure liquid radiochromatography was used to separate ^{18}F-FDHT from radiolabeled metabolites. Lesion-by-lesion comparisons between the ^{18}F-FDHT, ^{18}F-FDG, and conventional imaging methods were performed. **Results:** Metabolism of ^{18}F-FDHT was rapid, with 80% conversion within 10 min to radiolabeled metabolites that circulated bound to plasma proteins. Tumor uptake was rapid and tumor retention was prolonged. Fifty-nine lesions were identified by conventional imaging methods. ^{18}F-FDG PET was positive in 57 of 59 lesions (97%), with an average lesion maximum standardized uptake value (SUV_{max}) = 5.22. ^{18}F-FDHT PET was positive in 46 of 59 lesions (78%), with the average positive lesion SUV_{max} = 5.28. Treatment with testosterone resulted in diminished ^{18}F-FDHT uptake at the tumor site. **Conclusion:** ^{18}F-FDHT localizes to tumor sites in patients with progressive clinically metastatic prostate cancer and may be a promising agent to analyze antigen receptors and their impact on the clinical management of prostate cancer.

Key Words: 16β-^{18}F-fluoro-5α-dihydrotestosterone; PET; prostate cancer; androgen receptor

J Nucl Med 2004; 45:366–373

Prostate cancer is the second most common cause of cancer-related deaths in the United States (*1*). Several aberrant pathways contribute to the development of the metastatic phenotype and the emergence of castration resistance, which eventually lead to death of the patient. Clinically, virtually all patients show elevations in prostate-specific antigen (PSA) and evidence of continued signaling through the androgen receptor (AR). Pathologic and molecular analyses show evidence of AR gene expression and increased protein mutation, all of which contribute to a change of function, and ligand-independent activation (*2–7*). To effectively study the biology of prostate cancer and to develop therapies that target the AR require methods of assessing AR expression and functionality. However, such analyses are difficult as the dominant site of metastases is bone, a difficult site to biopsy. Furthermore, the biology of the metastases can differ from the primary prostate cancer; therefore, tissue from the primary tumor does not necessarily inform as to the status of the bony disease.

We have been developing molecular imaging techniques for the assessment of these pathways in prostate cancer. Dihydrotestosterone (DHT) is the primary ligand of the AR. Recently, Washington University (St. Louis, MO) has developed a radiotracer form of DHT, for the purpose of imaging AR expression noninvasively in vivo, using PET (*8,9*). This radiotracer form, 16β-^{18}F-fluoro-5α-dihydrotestosterone (^{18}F-FDHT), was selected for clinical research evaluation after comparison in animals with related compounds. In this article, we report on the initial studies of molecular imaging using the AR as a target.

MATERIALS AND METHODS

Patients

Patients were selected prospectively under a protocol that required that patients were castrate with evidence of disease progression according to laboratory and clinical criteria. Eligibility criteria included progressive histologically documented prostate cancer despite castrate levels (<50 ng/dL) of testosterone, progression as defined by a ≥50% increase in PSA that was sustained for a minimum of 3 observations obtained at least 1 wk apart, the development of new lesions, or an increase in preexisting lesions on bone scintigraphy. Patients were required to have a Karnofsky performance status of >60%. All patients were required to sign

Received June 20, 2003; revision accepted Oct. 29, 2003.

For correspondence or reprints contact: Steven M. Larson, MD, Department of Nuclear Medicine (SC212), Memorial Sloan-Kettering Cancer Center, 1275 York Ave., New York, NY 10021.

E-mail: larsons@mskcc.org

Downloaded from jnm.snmjournals.org by on March 14, 2017. For personal use only.

informed consent before registration to the study. As this protocol was an imaging study; there were no restrictions on concomitant therapies. However, care was taken so that no medications that directly competed for the AR were initiated before the ^{18}F-FDHT scans (except for posttherapy follow-up scans performed on 3 patients). Two of the patients were receiving chemotherapy regimens; 3 patients were on gonadotropin-releasing factor agonists while being prepared for therapies expected to alter AR expression or bioavailability (including treatment with the drug 17-allylamino-17-demethoxygeldanamycin [17-AAG] and high-dose testosterone); and the remaining 2 patients were on gonadotropin-releasing hormone agonist, goserelin (Zoladex) or leuprolide (Lupron) (Table 1), for the purposes of medical castration. The clinical trial was performed under the auspices of Memorial Sloan-Kettering Institutional Review Board, protocol IRB 97-007. ^{18}F-FDHT was administered under the auspices of the Memorial Sloan-Kettering Radioactive Drug Radioactive Drug Research Committee.

All 7 patients underwent ^{18}F-FDG PET, dynamic and whole-body ^{18}F-FDHT PET, and a bone scan. All patients had their ^{18}F-FDHT and ^{18}F-FDG PET scans within 48 h, except patient 6, who had an interval of 8 d because of ^{18}F-FDHT production problems.

The median age of the 7 patients was 66.5 y (range, 47–76 y), with a mean Karnofsky performance score of 85 (range, 80–90). The median baseline PSA was 69 ng/mL (range, 6.3−2,637 ng/mL), and the median testosterone concentration was 0 (range, 0–11 ng/dL). The median Gleason score was 7 (range, 7–10). Five of 7 patients had bone disease only, 1 patient had soft-tissue disease only, and 1 patient had both soft-tissue and bone disease.

Three of the patients were rescanned with ^{18}F-FDHT, 2 after treatment with exogenous testosterone and one after treatment with 17-AAG, an ansamycin derivative intended to degrade the AR. The follow-up ^{18}F-FDHT scan was performed 4–5 wk after the initial study. Two patients had pain and discomfort that precluded them lying in one position for a prolonged period. Therefore, dynamic scanning and kinetic analysis were not preformed on these patients.

Imaging Methodology

Before ^{18}F-FDG PET scanning, the patient was required to fast for at least 6 h, and a serum glucose determination was checked just before injection of 370 MBq (10 mCi) ^{18}F-FDG. All studies were performed with an Advance dedicated PET scanner (General Electric Medical Systems). This camera has a field of view of 55 cm in diameter and 15.2 cm in axial length. All scanning was performed in 2-dimensional (septa-in) mode. The transaxial resolution is 4.3-mm full width at half maximum (FWHM) at the center of the field of view, increasing to 7.3 mm at a radial distance of 20 cm. The average axial resolution decreases from 4.0-mm FWHM at the center to 6.6 mm at 20 cm (*10*). ^{18}F-FDHT scans were performed at least 24 h after the ^{18}F-FDG scan. No fasting was necessary. An index lesion was selected from the ^{18}F-FDG scan, and the patient was positioned within the scanner so that the index lesion was approximately in the center of the field of view. A transmission scan was performed first before administration of the ^{18}F-FDHT to verify correct positioning, and the patient was repositioned if necessary. The patient was injected through a central line and a 50-min dynamic emission scan was initiated. The dynamic scan was comprised of ten 1-min frames followed by eight 5-min frames. Upon completion of the dynamic scan, the patient was allowed to rest for 10 min and urinate if necessary. The patient was then repositioned on the couch, and a whole-body scan was performed from the bottom of the ear to the base of the pelvis. The emission scan was performed first (4 min per bed position) followed by the transmission scans of 3-min per bed position. All images were reconstructed by iterative reconstruction with segmented attenuation correction. The ^{18}F-FDHT and ^{18}F-FDG images were interpreted independently by one reader on a 5-point scale to categorize the confidence of detection of individual le-

TABLE 1
Comparison of ^{18}F-FDG and ^{18}F-FDHT Uptake in Patients with Advanced, Progressing Prostate Cancer

			^{18}F-FDHT		^{18}F-FDG	
Patient no.	Therapy*	Total no. of lesions	No. of positive lesions	SUV	No. of positive lesions	SUV
1	Leuprolide,† 17-AAG‡	7	3	5.70	7	7.40
2	Leuprolide†	9	5	3.45	9	4.70
3	Goserelin,† testosterone‡	16	15	4.73	16	4.56
4	Leuprolide†	4	4	3.30	4	4.63
5	Orchiectomy† Oral cyclophosphamide† Pamidronate† Celecoxib†	9	7	2.98	9	4.12
6	Leuprolide,† testosterone‡	6	4	6.53	4	4.05
7	Goserelin†	8	8	10.28	8	7.08
Total		59	46 (77%)	5.28§	57 (97%)	5.22§

*The generic name, trade name, manufacturer, and description are as follows: leuprolide (Lupron; TAP Pharmaceuticals USA), gonadotropin-releasing hormone analog; goserelin (Zoladex; Zeneca USA), gonadotropin-releasing hormone analog; cyclophosphamide (Cytoxan; Bristol MeyersSquibb USA), antineoplastic; pamidronate (Aredia; Novartis USA), bisphosphonate; celecoxib (Celebrex; Searle), nonsteroidal antiinflammatory.

†Baseline scan.

‡Follow-up scan.

§Mean.

Downloaded from jnm.snmjournals.org by on March 14, 2017. For personal use only.

sions. The studies were interpreted without knowledge of the bone scan, CT, or MRI findings. The scale was as follows: 1 = negative, 2 = probably negative, 3 = equivocal, 4 = probably positive, and 5 = definitely positive. The selection of a 5-point scale (rather than a 3-point scale) allowed the differentiation between clearly negative lesions (1) from probably negative (2), completely equivocal (3), highly suspicious (4), and definitely positive (5) lesions. This scale allowed a semiquantitative comparison of the confidence of the presence of tumor between ^{18}F-FDHT and ^{18}F-FDG. The comparative image reading of both tracers was performed using 2 triangulation display windows, which allowed transaxial, coronal, and sagittal slices of both image sets to be displayed alongside one another on a dual monitor. Lesions were delineated on the ^{18}F-FDG image set using a region-of-interest (ROI) tool, which is then copied to the corresponding lesion on the ^{18}F-FDHT image set. Only lesions that were scored 4 or 5 were considered positive for further analysis; therefore, the maximum standardized uptake value (SUV_{max}) is only reported for these lesions. SUV_{max} represents the maximum specific activity (Bq/g) of each tracer in the lesion divided by the injected activity (Bq) divided by the patient's weight (g). This is a quantitative scalar magnitude that is independent of the PET window display settings.

Radiochemical Synthesis of ^{18}F-FDHT

^{18}F was produced on the Memorial Sloan-Kettering Cancer Center CS-15 Cyclotron from the $H_2{}^{18}O$ by the $^{18}O(p,n)^{18}F$ nuclear reaction. An aliquot of the target water containing approximately 7.4 GBq (200 mCi) ^{18}F was added to nBu_4NOH (2.3 μL) contained in a vacuum-sealed test tube. The target water was removed with 3 azeotropic distillations using 0.5–1 mL of CH_3CN at an elevated temperature and a gentle stream of nitrogen. The dried activity was redissolved in tetrahydrofuran and transferred to a vacuum-sealed test tube containing 1–2 mg of triflate precursor, capped with a Teflon-lined stopper (DuPont), and placed in an oil bath at 55°C for 5 min. The mixture was subsequently cooled at −78°C. To the cold solution was added 0.150 mL of $LiALH_4$ solution (1 mol/L in Et_2O), mixed in a vortex, and allowed to react for 10 min before being quenched by the addition of 0.2 mL of acetone and 0.5 mL of 3N aqueous HCl. After a 10-min reaction period at 70°C, the contents were extracted with Et_2O 3 times and subsequently dried over anhydrous $MgSO_4$ and passed through a Na_2SO_4 drying column using ether. The ether was evaporated under vacuum and the residue was dissolved in 1 mL of high-pressure liquid chromatography (HPLC) solvent. The product was separated by normal-phase HPLC as previously described (*11*) with the no-carrier-added ^{18}F-FDHT formulated in 0.9% Sodium Chloride for Injection USP and Alcohol USP. The inactive components consisted of 0.9% Sodium Chloride for Injection USP and Alcohol USP in a ratio of 90:10 with a total volume of 5 mL for formulation.

The total radiochemistry synthesis time was approximately 100 min, and the ^{18}F-FDHT was produced in decay-corrected radiochemical yield approaching 30%.

Radiometabolite Analysis of ^{18}F-FDHT

Four patients who underwent an ^{18}F-FDHT scan had blood drawn for metabolite analysis. Up to a maximum of 17 serial blood samples were taken at the following collection times when possible: 0, 0.5, 1, 1.5, 2, 3, 4, 5, 7, 10, 15, 20, 30, 40, 50, 60, and 120 min after injection. Aliquots of blood were transferred in preweighed tubes and counted for activity. The remaining blood was centrifuged (5 min, 2,000*g* at room temperature), and aliquots of plasma were transferred into preweighed tubes and counted for activity in an LKB Wallac γ-counter (1282 Compugamma CS). The measured activities were corrected for decay, and data were expressed as SUV normalized to body weight.

To measure the fraction of free ^{18}F-FDHT versus protein-bound ^{18}F-FDHT, plasma samples were deproteinized by ultrafiltration. Therefore, 500 μL of plasma were transferred into prewashed filtration cartridges (Centricon YM-30; Millipore) and centrifuged according to the manufacturer's instructions. The filtrate was removed, weighed, and counted immediately in an LKB Wallac γ-counter (1282 Compugamma CS). The obtained activity per gram of the free fraction was corrected for decay and expressed as the percentage of the activity per gram from the corresponding plasma sample.

Metabolite analysis was determined by HPLC. One-half milliliter of plasma was mixed with 0.7 mL of acetonitrile containing unlabeled FDHT (0.05 mg/mL) as reference compound. After centrifugation at 2,000*g* for 5 min, the protein-free supernatant (about 1.1 mL) was removed, concentrated under reduced pressure, and used directly for the chromatographic evaluation. The HPLC system consisted of 2 pumps (model 501; Waters), a reversed-phase C_{18} column (Beckman Ultrasphere; 5 mm, 250 × 4.6 mm) connected to an ultraviolet detector (model 486; Waters) operated at 254 nm followed by a radioisotope detector (Radiomatic 625TR, 500 μL cell; Packard) and a fraction collector (FRAC-100; Pharmacia). The column was eluted applying a gradient from 40% acetonitrile in 0.01 mol/L phosphoric acid up to 90% acetonitrile using a flow rate of 1 mL/min and a run length of 20 min for each sample. Under these conditions, ^{18}F-FDHT elutes at 9 min. The data are expressed as the percentage of total activity in plasma. Fractions were collected and counted to calculate the recovery.

RESULTS

Imaging

A lesion-by-lesion comparison of the 59 individual lesions with regard to ^{18}F-FDG and ^{18}F-FDHT uptake was performed and a summary of all findings is summarized in Table 1. All of the bone lesions (detected by ^{18}F-FDG) were positive on bone scan, and the remaining soft-tissue lesions were positive on CT (Table 2), with the exception of 2 prostate bed recurrences. Combining the findings of all 7

TABLE 2
Results of Conventional Imaging Examinations in Patients with Advanced, Progressing Prostate Cancer

Patient no.	Total no. of lesions	No. of positive lesions		
		On bone scan	On CT	On MRI
1	7	0	7	1
2	9	8	2	NA
3	16	16	NA	NA
4	4	4	NA	NA
5	9	9	1	NA
6	6	6	1	NA
7	8	6	NA	NA

NA = not available.

Downloaded from jnm.snmjournals.org by on March 14, 2017. For personal use only.

patients in this study, 10 soft-tissue lesions and 49 bone lesions were detected. The number of lesions per subject varied from 4 to 16. The majority of the mismatched lesions, 8 of 11, were clustered in patients 1 and 2. ^{18}F-FDG was positive in 57 of 59 lesions (97%), with the average positive lesion SUV_{max} = 5.22. ^{18}F-FDHT was positive in 46 of 59 lesions (78%), with the average positive lesion SUV_{max} = 5.28.

An example of a typical ^{18}F-FDHT biodistribution (patient 6) is shown in Figure 1. The image is displayed in maximum-intensity-pixel (mip) format to allow full visualization of the biodistribution of the ^{18}F-FDHT tracer. Of particular note is the presence of ^{18}F-FDHT in the blood pool of the heart, great vessels, uptake in the vessels of the hand (of unknown cause) near the site of injection, concentration in the liver, and excretion of metabolite into the small and large intestine, especially excretion of the ^{18}F-FDHT via the bile (prominent gallbladder and bile ducts). There is uptake evident in metastatic tumor sites in the skull, right upper humerus, right axillary region (probably in a rib), and in left scapula. More posterior lesions, in the ischium and T10, are not well seen in this imaging format.

Figure 2 shows another ^{18}F-FDHT PET image (Fig. 2A) alongside the ^{18}F-FDG PET image (Fig. 2B) for patient 7. It illustrates the contrasting metabolism of the 2 tracers. As with patient 6, blood-pool activity is clearly apparent as is the gallbladder and biliary tree. In addition, there is uptake in numerous metastatic lesions in the cervical spine, left rib cage in 2 ribs, and left periaortic region. The large area of uptake in the pelvis could be confused with right iliac uptake, but the uptake is actually in an iliac loop, related to a urinary diversion, which the patient has undergone. There is uptake at the same sites on the ^{18}F-FDG images, although quantitative differences are apparent, in terms of the intensity of uptake. For example, the cervical lesion, though clearly ^{18}F-FDG positive, is less well seen than on the ^{18}F-FDHT image.



FIGURE 1. ^{18}F-FDHT scan of patient 6 (Table 1) displayed in mip format to allow better visualization of the whole-body distribution of this tracer. There is uptake in the skull, right upper humerus, and upper thorax at 2 sites.

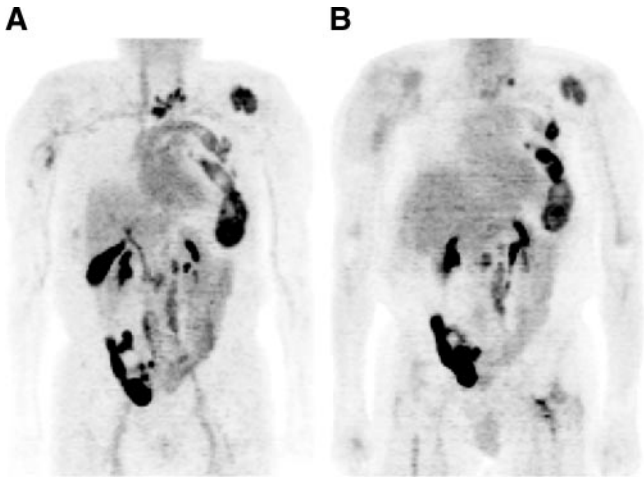


FIGURE 2. ^{18}F-FDHT (A) and ^{18}F-FDG (B) of patient 7 (Table 1) displayed in mip format.

Patient 1 underwent biopsy of the prostate bed recurrence, 13 d after a positive ^{18}F-FDHT study, at the site. The biopsy was positive for prostate cancer recurrence with a Gleason lesion score of 9/10. The histologic section (Fig. 3) shows clearcut AR expression or overexpression in the nuclei of the prostate cancer cells (brown stain) as they invade the blue-staining seminal vesicle cells. The brown stain reflects AR expression and illustrates the concept that AR staining in the nucleus is thought to represent active receptor.

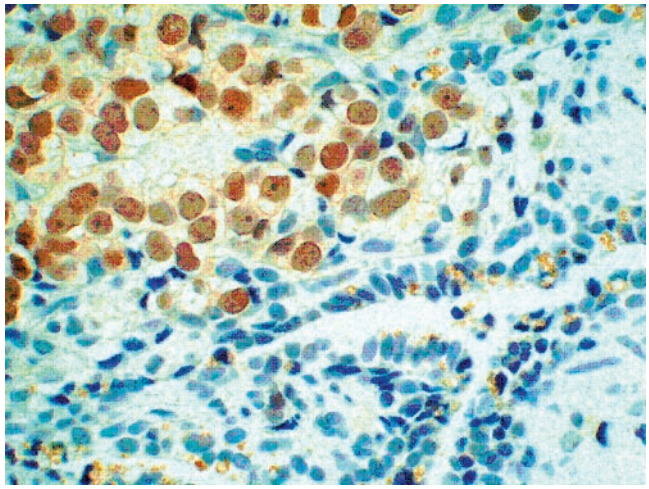


FIGURE 3. Prostate tumor section from a biopsy sample obtained from patient 1 stained with hematoxylin–eosin and also showing positive for androgen by immunohistochemistry (brown stain).

Downloaded from jnm.snmjournals.org by on March 14, 2017. For personal use only.

Pharmacokinetics

Four patients had blood drawn over the 60 min after injection. Plasma was separated, and analysis of protein-bound radioactivity and the proportion of radioactivity and metabolites were determined, after extraction with alcohol. The results for these 4 patients are shown in Figures 4A–4D.

Two patients had complete tumor uptake curves in 3 lesions before and after therapy. One such case is shown in Figures 5A and 5B. Uptake was rapid, with 80% of the final uptake occurring within 10 min. There was a prolonged plateau thereafter, during which time there was retention throughout the interval of study, with little discernible increase or loss in this plateau phase.

Blood clearance of ^{18}F-FDHT was determined by serum analysis (Fig. 4). The free fraction of activity in plasma was $<$2% at all time points during the investigation for patients 5, 6 (first ^{18}F-FDHT scan), and 7, indicating that ^{18}F-FDHT as well as the metabolic products are highly bound to plasma proteins. The only exception was found in patient 6 for the second ^{18}F-FDHT scan, where the free fraction was 95% and 30% for the 0.5- and 1-min plasma sample, respectively. This might be due to saturation of the peripheral DHT binding sides as a result of the testosterone treatment.

HPLC analysis of plasma samples shows a very fast metabolism of the radiotracer. The calculated in vivo half-lives were 4.2 min (patient 7), 3.5 min (patient 5), 5.8 min (patient 6, first administration), and 5.8 min (patient 6, second administration). The metabolic profile in all 4 subjects shows that the metabolites are more hydrophilic compared with those of ^{18}F-FDHT. However, in the subject with the fastest metabolism, additional more lipophilic metabolites are seen. These more lipophilic metabolites account for 75% in the 5-min plasma sample and drop to 5% in the 30-min plasma sample. They are below the detection limit in all later plasma samples. Values for the recovery of the samples from HPLC were measured and were always $>$95%, indicating that no lipophilic metabolites were missed due to the selected elution conditions. Therefore, it must be assumed that the in vivo metabolism of ^{18}F-FDHT can vary somewhat between subjects but is uniformly rapid.

Posttreatment Effects on Uptake

Three patients had follow-up scans after treatment. Two received exogenous testosterone (patients 3 and 6 in Table

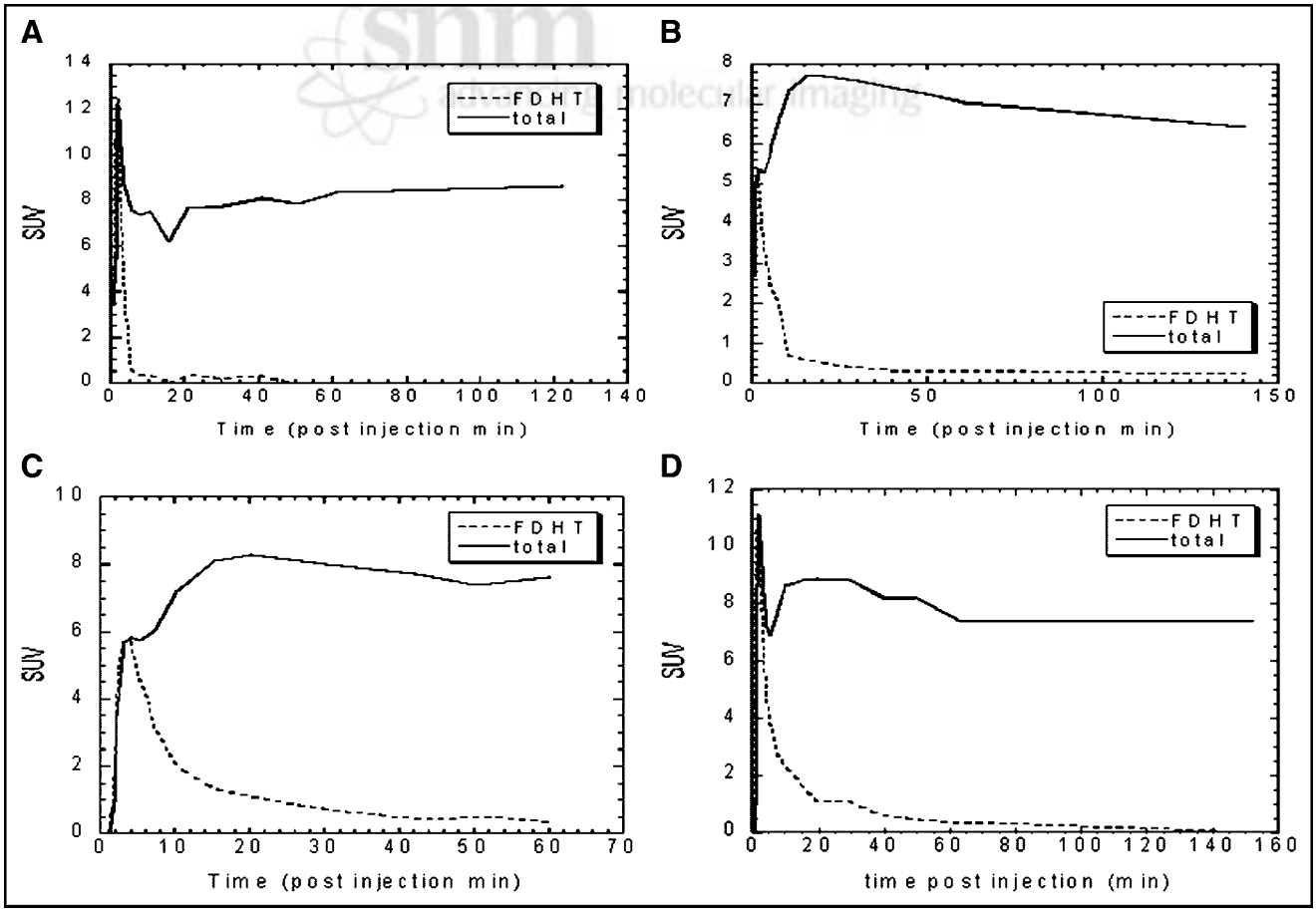


FIGURE 4. Fraction of ^{18}F-FDHT vs. total ^{18}F activity from blood samples of 4 patients (A–D), who had repeated blood samples drawn over the 60 min after injection.

Downloaded from jnm.snmjournals.org by on March 14, 2017. For personal use only.

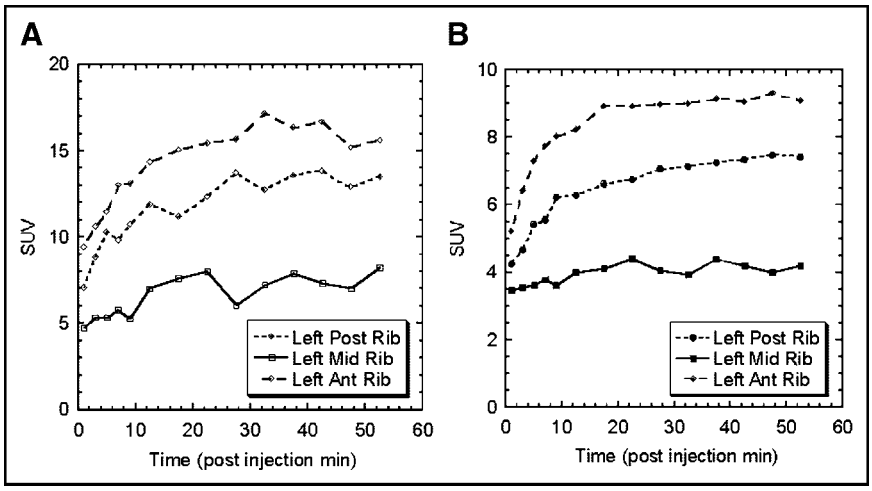


FIGURE 5. ^{18}F-FDHT tumor uptake in each of 3 lesions of patient 7 obtained by ROI analysis from the dynamic PET data before (A) and after (B) therapy. Post = posterior; Mid = middle; Ant = anterior.

1) and patient 1 received ansamycin (17-AAG). Both of these types of treatments would be expected to reduce the binding of ^{18}F-FDHT to the AR. Testosterone treatment should increase the amount of DHT competing at the receptor site, and this should reduce uptake. 17-AAG should reduce the concentration of the AR itself, through its action on heat shock protein-90 (*12*).

A coronal and axial image shows the sites of the lesion in patient 3 (Fig. 6 top). The ROI analysis of these 3 lesions on the dynamic PET datasets is also shown in Figure 6 (bottom) for scans before and after therapy. In this patient, the DHT concentration increased from a baseline level of 3 ng/dL to a value of 62 ng/dL at the time of second study. In the posttreatment scan, the ^{18}F-FDG scans showed no significant change, either in the number of lesions or the SUV level, before and after therapy. The average SUV1 = 4.56 (n = 16); the average SUV2 = 4.37 (n = 16). There was a major reduction in ^{18}F-FDHT uptake in the 3 tumors for which time–activity curves were available, and the whole-body images showed a visual reduction in uptake in all 15 lesions that were initially positive with ^{18}F-FDHT.

The second patient treated with testosterone had a documented elevation in serum DHT of 54 ng/dL, but this decreased to 2 ng/dL before the follow-up ^{18}F-FDHT scan. The ^{18}F-FDG scans showed no significant change from the pretherapy scan (average SUV of 4.05 [n = 5] before therapy vs. 4.06 [n = 5] after therapy). The follow-up ^{18}F-FDHT study was essentially unchanged from the baseline, suggesting that it is the ambient concentration of hormone—not the prior history of treatment—that determines ^{18}F-FDHT tracer localization.

A third patient (patient 1) was treated with 17-AAG, and both ^{18}F-FDG and ^{18}F-FDHT scans were repeated after therapy. The ^{18}F-FDG scans showed only a slight change (average SUV of 7.5 [n = 7] before therapy vs. 8.8 [n = 9] after therapy]). Two new lesions, one in the right iliac crest and another in the cervical spine, had avid ^{18}F-FDHT and ^{18}F-FDG uptake (Fig. 7).

The data from the 3 patients imaged with ^{18}F-FDHT after therapy support the concept that there is competition between ^{18}F-FDHT and DHT for the AR in the tumor sites and also that the uptake of ^{18}F-FDHT in lesions does reflect posttreatment changes in the AR levels.

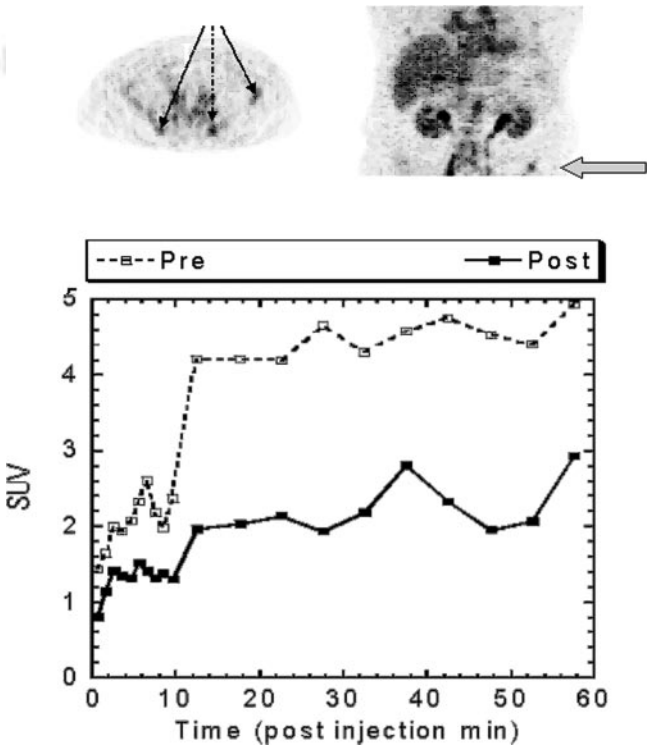


FIGURE 6. (Top) Coronal and transaxial image displays containing 3 tumor sites in the pelvis (left iliac crest, the left and right sacroiliac joints) on which ROIs were drawn. (Bottom) Time–activity curves before (dashed line) and after (solid line) treatment with testosterone. The ordinate values represent an average of all 3 lesion SUVs for clarity, although all 3 tumors showed significant suppression of ^{18}F-FDHT uptake after treatment.

Downloaded from jnm.snmjournals.org by on March 14, 2017. For personal use only.

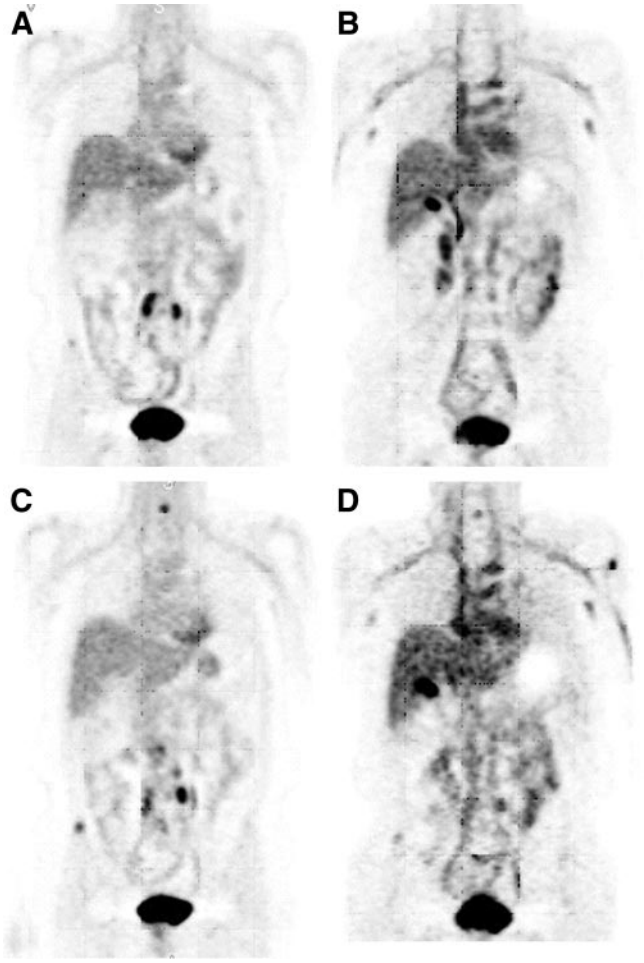


FIGURE 7. ^{18}F-FDG and ^{18}F-FDHT images of patient 1 before and after treatment with 17-AAG. (A and B) Corresponding coronal sections from the pretreatment ^{18}F-FDG and ^{18}F-FDHT scans. (C and D) Respective coronal slices after therapy. New lesions are seen on ^{18}F-FDG and ^{18}F-FDHT in the ilium, C3, and prostate bed. The site in the prostate bed was confirmed by biopsy.

DISCUSSION

This study was performed to investigate the potential of a new radiotracer, ^{18}F-FDHT, to characterize the biology in terms of the androgen levels of patients with prostate cancer. Direct tissue samples are not part of routine clinical practice for metastatic prostate cancer and are, in many cases, difficult or impossible to obtain. The patterns of spread of prostate cancers make it difficult to quantify tumor regression and progression in a reproducible way. Most patients with advanced disease have bone metastases, and the radionuclide bone scan is a sensitive means for detecting initial spread to bone (*13*), but this method does not visualize tumor directly and exhibits a significant lag when used to assess acute tumor response (*14*).

These difficulties with conventional single-photon nuclear techniques have resulted in the exploration of ^{18}F-FDG PET (*15*) for the detection of metastatic prostate cancer, and there is emerging evidence that such approaches will be useful for monitoring treatment response in solid tumors as well (*15–17*). However, the role of ^{18}F-FDG PET in prostate cancer is controversial, and the results are heavily influenced by the patient selection. At our center, a disease-states model is used to control patients for a discrete phase in the natural history of the disease (*18,19*). Our selected patient population has shown that lesions seen on bone scan only remain stable over time, whereas lesions seen on ^{18}F-FDG PET progressed (*20*).

In this study, we applied similar stringent criteria for selecting patients eligible for the ^{18}F-FDHT protocol. ^{18}F-FDHT is a selective marker for ARs and, therefore, exhibits prostate cell specificity. In this way, it is a more direct measure of prostate metastases than the bone scan (or even ^{18}F-FDG).

In the 7 patients studied, we identified 57 ^{18}F-FDG–avid lesions in bone and soft tissue that correlated with suspicious findings on bone scintigraphy, CT, or MRI. Seventy-nine percent of these ^{18}F-FDG–avid lesions also took up ^{18}F-FDHT. The purpose of this study was to identify a group of metabolically active tumor sites that could be assessed in terms of their ability to take up and retain ^{18}F-FDHT. Correspondence between ^{18}F-FDHT with ^{18}F-FDG was found in 5 of 7 patients. Two of the patients accounted for the majority of mismatched lesions, which were ^{18}F-FDG–positive, ^{18}F-FDHT–negative lesions. The basis for this metabolic heterogeneity is unknown but is hypothesized to represent variability in AR status versus glucose metabolic rate. Such differences may underscore the biologic heterogeneity of prostate cancer that occurs during disease progression. Follow-up studies to further explore these relationships are being undertaken in the laboratory and the clinic. The results of properly controlled clinical trials show that there is continued AR signaling in the overwhelming majority of castrate patients and, therefore, that AR is a relevant therapeutic target.

In all subjects for whom adequate data were available, the metabolism of ^{18}F-FDHT was rapid, with 80% conversion within 10 min to a radiolabeled metabolite that circulated bound to plasma proteins. Tumor uptake was also rapid (80% uptake at 10 min), suggesting that ^{18}F-FDHT was the active radiopharmaceutical for targeting, and entered a plateau phase for the duration of the dynamic and subsequent whole-body scan, indicating tumor cell retention. Tumor SUV values for ^{18}F-FDHT were in the same range as for the initial scans on all patients, suggesting that the rapid metabolic half-life did greatly affect individual lesion uptake. Instead, biologic features of the tumor, such as the AR, are the likely cause for the finding that some tumors had excellent uptake.

CONCLUSION

To our knowledge, this study is the first assessment of PET scanning to characterize castrate metastatic prostate lesions, in patients with progressive disease visible by con-

Downloaded from jnm.snmjournals.org by on March 14, 2017. For personal use only.

ventional imaging methods, on the basis of the AR. We have shown that imaging prostate cancer by ^{18}F-FDHT PET is feasible and that sites of uptake correspond with sites demonstrated by standard bone scintigraphy, soft-tissue imaging, and ^{18}F-FDG PET. A major finding of this study was that, of the 59 lesions detected in 7 patients, the majority of metastatic lesions also demonstrated ^{18}F-FDHT uptake. A second important observation was that, although many tissues in the body would be expected to exhibit AR expression, prostate cancer bound tracer with far greater affinity than normal tissue. This finding allows the identification of active disease, lending credence to the observation that the AR is overexpressed in androgen-independent metastatic disease.

The data from this initial study will be used to generate hypotheses for further testing. Questions raised by our findings include the following: What is the correlation between ^{18}F-FDG avidity, ^{18}F-FDHT avidity, and treatment response of individual lesions? What is the relationship between lesions seen by standard imaging studies and ^{18}F-FDHT uptake. What is the relationship between ^{18}F-FDHT uptake and AR expression as assessed by immunohistochemistry. A separate clinical trial in which ^{18}F-FDHT is being compared with ^{18}F-FDG PET and with pathologic assessments of the AR is now underway.

ACKNOWLEGMENTS

The authors thank Dr. Victor Reuter, of the Pathology Department, Memorial Sloan-Kettering Cancer Center, for providing the immunohistology shown in Figure 3. Also, special thanks go to John Katzenellenbogen from the University of Illinois, Urbana, for his continued intellectual input and support of this study. The authors also thank Rebecca Gonzalez and Elaina Chu for assisting in the gathering of scan- and patient-related data. This research was supported in part by the Norman Hascoe Fund, the Laurent and Alberta Gerschel Foundation, and National Cancer Institute grant P50 CA 86438.

REFERENCES

1. Jemal A, Murray T, Samuels A, Ghafoor A, Ward E, Thun MJ. Cancer Statistics, 2003. *Cancer J Clin.* 2003;53:5–26.
2. Horst T, Meyer B, Taplin S. Screening, health promotion, and prevention in men. *Prim Care.* 1995;22:679–695.
3. Fenton MA, Shuster TD, Fertig AM, et al. Functional characterization of mutant androgen receptors from androgen-independent prostate cancer. *Clin Cancer Res.* 1997;3:1383–1388.
4. Craft N, Sawyers CL. Mechanistic concepts in androgen-dependence of prostate cancer. *Cancer Metastasis Rev.* 1998;17:421–427.
5. Visakorpi T, Hyytinen E, Koivisto P, et al. In vivo amplification of the androgen receptor gene and progression of human prostate cancer. *Nat Genet.* 1995;94: 401–406.
6. Koivisto P, Visakorpi T, Rantala I, et al. Increased cell proliferation activity and decreased cell death are associated with the emergence of hormone-refractory recurrent prostate cancer. *J Pathol.* 1997;183:51–56.
7. Agus DB, Cordon-Cardo C, Fox W, et al. Prostate cancer cell cycle regulators: response to androgen withdrawal and development of androgen independence. *J Natl Cancer Inst.* 1999;91:1869–1876.
8. Bonasera TA, O'Neil JP, Xu M, et al. Preclinical evaluation of fluorine-18-labeled androgen receptor ligands in baboons. *J Nucl Med.* 1996;37:1009–1015.
9. Choe YS, Lidstrom PJ, Chi DY, et al. Synthesis of 11 beta-[^{18}F]fluoro-5 alpha-dihydrotestosterone and 11 beta-[^{18}F]fluoro-19-nor-5 alpha-dihydrotestosterone: preparation via halofluorination-reduction, receptor binding, and tissue distribution. *J Med Chem.* 1995;38:816–825.
10. Degrado TR, Turkington TG, Williams JJ. Performance characteristics of a whole-body PET scanner. *J Nucl Med.* 1994;34:1348–1406.
11. Liu A, Dence C, Welch MJ. Fluorine-18-labeled androgens: radiochemical synthesis and tissue distribution studies on six fluorine-substituted androgens, potential imaging agents for prostatic cancer. *J Nucl Med.* 1992;33:724–734.
12. Solit DB, Zheng FF, Drobnjak M, et al. 17-Allylamino-17-demethoxygeldanamycin induces the degradation of androgen receptor and HER-2/neu and inhibits the growth of prostate cancer xenografts. *Clin Cancer Res.* 2002;8:986–993.
13. Larson, SM, Schwartz LH. Advances in imaging. *Semin Oncol.* 1994;21:598–606.
14. Smith PH, Bono A, Calais da Silva F. Some limitations of the radioisotope bone scan in patients with metastatic prostatic cancer: a subanalysis of EORTC trial 30853—the EORTC Urological Group. *Cancer.* 1990;6:1009–1016.
15. Shreve PD, Grossman HB, Gross MD, et al. Metastatic prostate cancer: initial findings of PET with 2-deoxy-2-[F-18]fluoro-D-glucose. *Radiology.* 1996;99: 751–756.
16. Fong Y, Saldinger PF, Akhurst T, et al. Utility of ^{18}F-FDG positron emission tomography scanning on selection of patients for resection of hepatic colorectal metastases. *Am J Surg.* 1999;78:282–287.
17. Pieterman RM, van Putten JW, Meuzelaar JJ, et al. Preoperative staging of non-small-cell lung cancer with positron-emission tomography. *N Engl J Med.* 2000;43:254–261.
18. Scher HI. Prostate carcinoma: defining therapeutic objectives and improving overall outcomes. *Cancer.* 2003;7(3 suppl):758–771.
19. Scher HI, Kelly WK. States and state transitions are all that really matter [editorial]. *J Urol.* 2002;168:2451–2453.
20. Yeh SDJ, Larson SM, Garza D, et al. Detection of bony metastases of androgen independent prostate cancer by PET-FDG. *Nucl Med Biol.* 1996;23:693–697.

Downloaded from jnm.snmjournals.org by on March 14, 2017. For personal use only.

JNM The Journal of NUCLEAR MEDICINE

Tumor Localization of 16β-^{18}F-Fluoro-5α-Dihydrotestosterone Versus ^{18}F-FDG in Patients with Progressive, Metastatic Prostate Cancer

Steven M. Larson, Michael Morris, Ilonka Gunther, Brad Beattie, John L. Humm, Timothy A. Akhurst, Ronald D. Finn, Yusuf Erdi, Keith Pentlow, Jon Dyke, Olivia Squire, William Bornmann, Timothy McCarthy, Michael Welch and Howard Scher

J Nucl Med. 2004;45:366-373.

This article and updated information are available at:
http://jnm.snmjournals.org/content/45/3/366

Information about reproducing figures, tables, or other portions of this article can be found online at:
http://jnm.snmjournals.org/site/misc/permission.xhtml

Information about subscriptions to JNM can be found at:
http://jnm.snmjournals.org/site/subscriptions/online.xhtml

The Journal of Nuclear Medicine is published monthly.
SNMMI | Society of Nuclear Medicine and Molecular Imaging
1850 Samuel Morse Drive, Reston, VA 20190.
(Print ISSN: 0161-5505, Online ISSN: 2159-662X)

© Copyright 2004 SNMMI; all rights reserved.

SNMMI SOCIETY OF NUCLEAR MEDICINE AND MOLECULAR IMAGING